UDC: 616-006.6-085.949.2.036.8
Original scientific paper

ANGULAR DISTRIBUTION OF NEUTRONS FROM PROTON AND CARBON ION THERAPY USING AHUBO PHANTOM (MONTE CARLO SIMULATIONS WITH FLUKA)

Redona IZAIRI-BEXHETI[1], Mimoza RISTOVA[1, 2*]

[1]Institute of Physics, Faculty of Natural Sciences and Mathematics, Ss Cyril and Methodius University in Skopje, Arhimedova 3, Skopje, North Macedonia
[2] SEEIIST, Southeast European International Institute for Sustainable Technologies, Geneva, Switzerland.
**Corresponding Author: e-mail: mima.ristova@gmail.com*

Abstract

Accelerated protons and C-ions are used by means of radiation therapy (RT) for cancer treatment for over 50 years. Monte Carlo simulations with FLUKA transport code were performed to simulate particle therapy with either protons or C-ions at a given radiation therapy energy. The average Human Body (AHUBO) Phantom has been used to create a human head model (sphere of 8 cm radius). The AHUBO head was placed in (0, 0, 0) the Cartesian system of the Flair graphical interface of FLUKA, and the ion source at Z=-30 cm apart from the centre. The primary beams consisted of 107 protons of 100 MeV and 107 C-ions with 190 MeV/u, energies pertaining to a Bragg peak positioned in the centre of the AHUBO head model (coinciding with the position of the pituitary). The Angular distribution of secondary neutrons with respect to the incident direction of the primaries was scored with a USRBDX for angles 0-180 degrees of solid angle (step 15 degrees). Results showed that there are three typical maxima in the neutron spectra, one thermal and two high energy (HE) peaks. The position and the intensity of the HE peaks change with the change of the solid angle for both incident particle type simulations. The neutron fluence near the margin of the 8 cm radius sphere (region inwards) for the treatment with primary protons was estimated to be in the range of 10-5cm-2, while in the case of treatment with primary C-ions, the fluence was one order of magnitude greater (10-4).

Keywords: Cancer, Radiation therapy, Proton therapy, C-ion therapy, neutrons, angular distribution, AHUBO phantom

1. Introduction

Cancer is a critical societal issue. Worldwide, in 2018 alone, 18.1 million cases were diagnosed, 9.6 million people died and 43.8 million people were living with cancer (Figure 1). Current projections anticipate an increase with approximately 24.6 million newly diagnosed patients and 13 million related deaths by 2030. Cancer imposes an enormous economic burden worldwide - around 2 trillion dollars in 2010 and these costs are rising and putting a major burden on public healthcare budgets. In the EU over 3.7 million new cases per year are diagnosed and total costs of over 120 billion EUR were reported for the EU in 2012. Combating cancer is considered a priority research challenge by the European Commission, this is particularly relevant in the Balkan region where mortality rates from cancer are on average 40% higher compared to the rest of Europe (M.M. Ristova, 2021)(M. Dosanjh, 2022)(U. Amaldi, 2021).

Radiation therapy (RT) aims to treat cancer cells with a dose of radiation sufficient to stop their growth, and because their cell death, while sparing the surrounding healthy tissue from damage (Baskar, 2012). Hadron therapy (HT) alternatively called particle therapy (PT) involves the pre-acceleration of hadrons (charged particles such as protons or heavier ions) to relativistic speeds. The ion beam is then subjected to targeting to the tumour volume according to the laws of ballistics, guided to the target by appropriate magnetic fields, which is a great advantage over classical RT with X-ray photons (Schulz-Ertner, 2007).

Thirty years after the design of the first generation of such facilities (Jones, 2005), the time has come for more rapid progress and a more intense breakthrough in the technologies of creating intense and precise

high-ion beams that will make the treatment of cancer with heavy-ion beams accessible to a larger part of the European population. After many years of experiments and clinical trials PT in cancer treatment has proven to be more convenient than conventional RT due to the significantly reduced radiation dose in healthy tissues surrounding the tumour (Janz, 2004) since it is characterized by highly conformal dose distributions.

In Figure 1we present the basis of hadron therapy using a two-dimensional cross-section of an elliptical model of healthy tissue with a circular morel of a tumour at the centre of the ellipse.

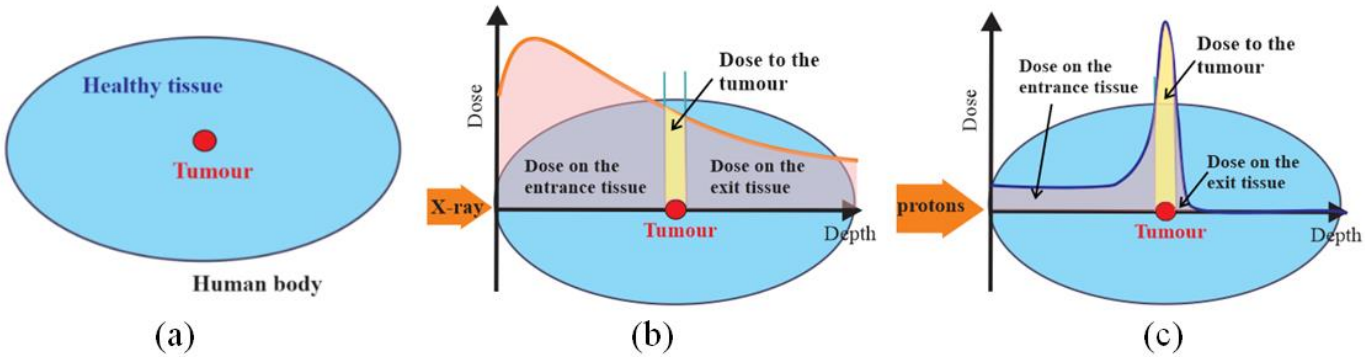

Figure 4. Comparison between dose distribution in target tumor and healthy tissue in a simplified 2D human body model(R.I.-Bexheti M. R., 2020).

Figure 1 (a) shows a transversal section of a human body model: healthy tissue (blue ellipse) with a tumour inside (red circle). Figure 1 (b) shows the dose distribution within the depth profile in classical RT X-ray treatment. The orange area on the left is proportional to dose delivered to healthy tissue at the entrance of radiation to the human body, the yellow area is the tumour dose and the orange area on the right is the dose to healthy tissue at the exit. Figure 1 (c) shows the dose distribution over depth in particle therapy (PT) with protons. Orange area on the left - dose delivered to the healthy tissue at the entrance, yellow area - tumour dose, orange area on the right - dose to the healthy tissue at the exit.

During particle therapy with protons and C-ions, secondary neutrons are generated as the primary beam interacts with the nuclei of the patient's tissues, causing further interactions and potential problems. The main challenges associated with neutron production in proton and carbon ion therapy are as follows: (a) Neutrons have a high relative biological effectiveness (RBE)(Paganetti, 2002), which means they can cause more damage to the surrounding healthy tissue than the primary beam, increasing the risk of occurrence of secondary cancers and other radiation-related unwanted effects; (b) Neutrons are produced in a random manner during the treatment, which makes them difficult to control and predict. This can affect the accuracy and precision of the treatment, which is crucial for cancer patients; (c) As neutral particles neutrons have a longer range than the primary beam of charged particles, which means they can travel beyond the intended treatment area and damage the healthy tissue in other parts of the body; (d) Neutron production can also increase the dose to the patient's skin, which can lead to skin stochastic reactions and other side effects; (e) Neutron production also poses a risk of overexposure of treatment staff to the secondary radiation during the treatment process(Islam, 2013). Various simulations should be implemented to address these problems to predict the fluence of neutrons created during the proton or C-ion therapy (Lindborg, 2013).

2. Methodology

Monte Carlo simulations

The Monte Carlo (MC) transport code is a technique for solving mathematical problems using random sampling, either those that are fully deterministic (e.g., estimation of an integral) or those of a stochastic nature (e.g. particle scattering). Although variants of MC methods can be traced back as far the 18th century, the fundamentals of the modern MC technique for solving stochastic problems were developed in the 1930s and 1940s(Kalos, 2009). Enrico Fermi in 1932, and Stanislaw Ulam together with John von Neumann in 1947 used the method to calculate neutron diffusion and multiplication (Cooper, 1987)(Islam, 2013). An MC simulation of particle transport and interaction is performed according to the following 4 major steps (Chetty, 2007): 1. Random selection of the distance to the next interaction, based on random sampling following the exponential path length distribution. The mean free path of this distribution is defined by the total cross section for the given particle and material properties; 2. Transport of the particle in the matter along a step to the interaction location, taking into account geometry constraints and the potential presence of electromagnetic fields; 3. Random selection of the interaction type according to the partial cross sections; 4. Simulation of the selected interaction and production of secondary's, with particle properties sampled from the corresponding distributions.

FLUKA code and Flair graphical interface

FLUKA[1] is a fully integrated particle physics Monte Carlo (MC) simulation package. It has many applications in high-energy experimental physics and engineering, shielding, detector and telescope design, cosmic ray studies, dosimetry, medical physics, and radiobiology (Battistoni, 2007).FLUKA is a general-purpose tool for calculations of particle transport and interactions with matter, covering an extended range of applications spanning from proton and electron accelerator shielding to target design, calorimetry, activation, dosimetry, detector design, accelerator driven systems, cosmic rays, neutrino physics, radiotherapy etc. (Fasso, 2003). It is said that simulations with MC is a "mathematical experiment". In other words, the MC is equivalent to the result of a real experiment (i.e., of measurement with detectors), herein called an estimator. Just like the real measurement, an MC estimator is obtained by sampling from a statistical distribution and has a statistical error and a systematic one (De Saint-Hubert, 2022). Several scoring (mathematical measuring) possibilities are available by means of SCORE cards. Via these cards, FLUKA can score particle fluence, current, track length, energy spectra, energy deposition, dose deposition, dose equivalent, etc. The possible detectors that can be used are USRTRACK and USRCOLL, USRBDX, USRBIN and USRYIELD.

In our simulations we have used USRBDX and USRBIN. Herein, the USRBDX score average $d^2\Phi/dEd\Sigma$(double-differential fluence (Φ) or current from the energy -log E and the solid angle - Σ) of a given type or family of particles on a given surface. USRBIN scores the spatial distribution of energy deposited, or total fluence in a regular mesh (cylindrical or Cartesian) defined by the user.

AHUBO phantom stoichiometry model

Simulations of clinical proton radiotherapy treatment plans are using general-purpose Monte Carlo codes that have been proven to be valuable tools for basic research and clinical studies. Medical calculation methods, on the other hand, are based on actual experimental data as a reference model. It is crucial that the Monte Carlo results closely match a clinical algorithm in such reference conditions (Parodi, 2007). The

[1]http://www.fluka.org/fluka.php

uncertainties that exist in the physics models describing the transport and interaction of the protons can, however, exceed the maximum acceptable difference (Pia, 2010). Therefore, considering these limitations, simulation methods need to be designed so that the uncertainties in the models and parameters are cancelled out or compensated for appropriate empirical adjustments.

For the purposes of this study, we utilized our previously developed atomic stoichiometry model of a human body phantom (AHUBO) composed of a homogeneous mixture of the elements that are presented with a mass content better than 0.2%(Bexheti, 2023), that was made under the assumption that an average human body is comprised of the following elements in atomic compound stoichiometry percentages: oxygen (O) – 24%; carbon (C) - 12%;hydrogen (H) - 62% is; nitrogen (N) – 1.1%; calcium (Ca) – 0.22%. It's used as a structural material in bones, but it is essential for protein regulation and muscle contraction; phosphorus (P) – 0.22%.

In our FLUKA simulations, we have used a 3D AHUBO stoichiometry model phantom, with a spherical geometry of 8 cm radius, emulating human head (blue ellipse in our projection), placed in the X,Y, Z (0,0,0) (also the isocenter), as presented in Figure 1. Figure 2presents the AHUBO phantom's position in the air. The proton/ion source (blue) was placed at -30 cm from the centre along the Z-direction. The primary beams consisted of either 107 protons of 100 MeV or C-ions with 190 MeV per nucleon, both the energies previously found to produce Bragg peaks positioned in the vicinity of the isocenter X(0,0,0) of the AHUBO head model, emulating, for instance, the case of irradiating pituitary gland.

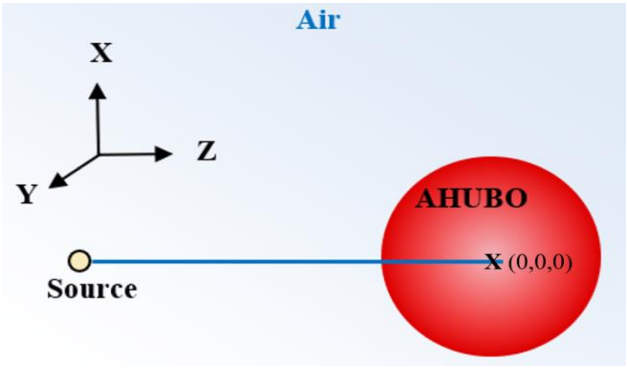

Figure 2. Graphical presentation of the simulation geometry of sphere emulating human head (AHUBO Target) and a source of monochrome ion energies 100 MeV for protons or190 MeV/u for C-ions, with isocenter in X (0,0,0).

Neutron production

The incident primary particles (protons or C-ions) in collision with the target nuclei interact with inelastic scattering. In the energy exchange process, neutrons with different energies from that of the incident are produced. The resulting neutron spectrum during particle therapy depends on the energy and type of the primary particle beam, as well as the characteristics of the target tissue. Typically, the neutron spectrum (energy distribution) is ranging from parts of an eV to several hundreds of MeV. Most of the neutrons produced during particle therapy have peak energies in the range of a few tens of eV to a few hundred MeV (Howell, 2014). The low-energy neutrons are known as thermal neutrons (ranging from several parts of an eV to 1 keV) and have a longer mean free path in tissue compared to higher-energy neutrons. This means that they can travel further through the tissue and deposit energy at greater distances from the primary particle beam. As the incident particle interacts with the target material, secondary particles may be emitted in different directions, leading to a particular angular distribution.

The neutron spectrum also contains fast neutrons with energies in the range of a few hundred keV to several MeV. These neutrons can contribute to the overall dose received by the patient by the surrounding healthy tissues. The neutron spectrum produced during particle therapy with protons and C-ions) is an important

consideration in treatment planning, as it can affect the effectiveness and safety of the treatment. In particular, the production of neutrons can increase the risk of the appearance of secondary cancers and other radiation-induced side effects. Also, these neutrons should be taken into consideration when evaluating the exposure of the staff in the particle therapy treatment centers, and the dose from the isotopes that are generated in the apparatus and bunker shielding materials from the neutron's interactions with the matter. Therefore, the neutron spectra and their angular distribution, by means of fluence or its double differential as a function of their energy is an important challenge for estimation with MC tools.

3. Results and discussion

For this study we have selected the energies of the primary particles to correspond to the energy at which the Bragg-peak falls in the isocenter of the AHUBO phantom, located at XYZ (0,0,0), also coinciding with the center of the sphere with radius 8 cm. The Figure 3 presents the energy deposition (dE/dx) in the depth of the phantom, with clearly distinct Bragg-peaks resulting from primary protons of 100 MeV (red curve) and primary C-ions of 190 MeV (blue curve), targeting the isocenter at XYZ(0,0,0) of the AHUBO phantom. The particle ranges in the depth (Z-direction) are also presented in Figure 3.

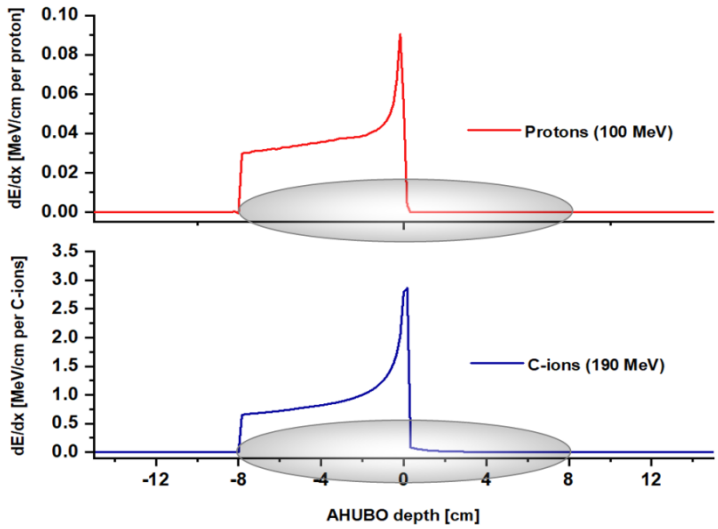

Figure 3. Bragg-peaks of primary protons (100 MeV) and primary C-ions (190 MeV) targeting the isocenter at XYZ(0,0,0) of the AHUBO phantom, and the range in the depth (Z-direction). Gray shaded ellipse represents the phantom geometry for illustration purposes.

From Figure 3 it is evident that the linear energy transfer (dE/dx) at approximately -4 cm (halfway to the isocenter) from the entrance of the primary beam in the AHUBO is about 0.035 for protons and 0.8 for C-ions. This indicates that the linear energy transfer for C-ions is about 23 times higher than that of protons.

Simulation of neutrons distribution with primary protons of 100 MeV

Figure 4 illustrates the double differential angular distributions of neutrons as a function of energy, obtained by plotting the angular distribution with respect to the collision direction using a USRBDX for angles ranging from 0 to 180 degrees of solid angle, with a step size of 15 degrees caused by incident primary protons of 100 MeV. Herein we present the angular distributions within solid angle ranges within 0 to 90 degrees (step 15 degrees) with respect to the incident beam direction (Z-axis). The main figure on 4(a) pertains to the angular distribution of energy of neutrons within the solid angle 0-15 degrees with respect to

the incident direction. The spectrum exhibits two distinct peaks - the first corresponding to the thermal neutron region (light blue) with energy of 0.06 eV, while the second one to fast neutron one with high energy (HE) (light red) at 21 MeV. One can also notice that the high energy region peak also reveals a small overlapping peak at 3.01 MeV. In addition to these peaks, there exists an intermediate energy continuum of neutrons between them. The spectra obtained by other authors (Howell, 2014) who have experimentally with real patient treatments used a primary proton beam of 250 MeV also contained three distinct peaks: one in the region of thermal neutrons located at 0.6 eV and two fast neutrons, one located at around 12.5 MeV (originating from evaporation neutrons) and at about 60 MeV (direct neutrons). The small figure within 3 (a) presents the neutron spectra in other spatial angle regions for angles between 15 and 90 degrees. Herein, the peak energies are shifted towards smaller energies (range of several MeV). Figure 4 (b) displays the neutron spectra for solid angles ranging from 90 to 180 degrees (step 15 degrees) from the direction of the incident particles. Again, the thermal region exhibited a distinct peak at 0.06 eV evident for all angle ranges. In the region of fast neutrons (HE), a peak was observed at about 5 MeV. Another peak is evident in the intermediate energy region at 3 keV.

One may conclude that there is an obvious energy shift of the maxima in the spectra towards the smaller energies with the growing spatial angle from the incident particle direction. Also, it is evident that the double differential of the fluence dramatically drops (for over two orders of magnitude) for solid angle regions other than those 0-15 degrees. Hence, the high-energy neutrons resulting from proton interactions have their preferential direction of the incident primary protons (main chart in Figure 4(a)).

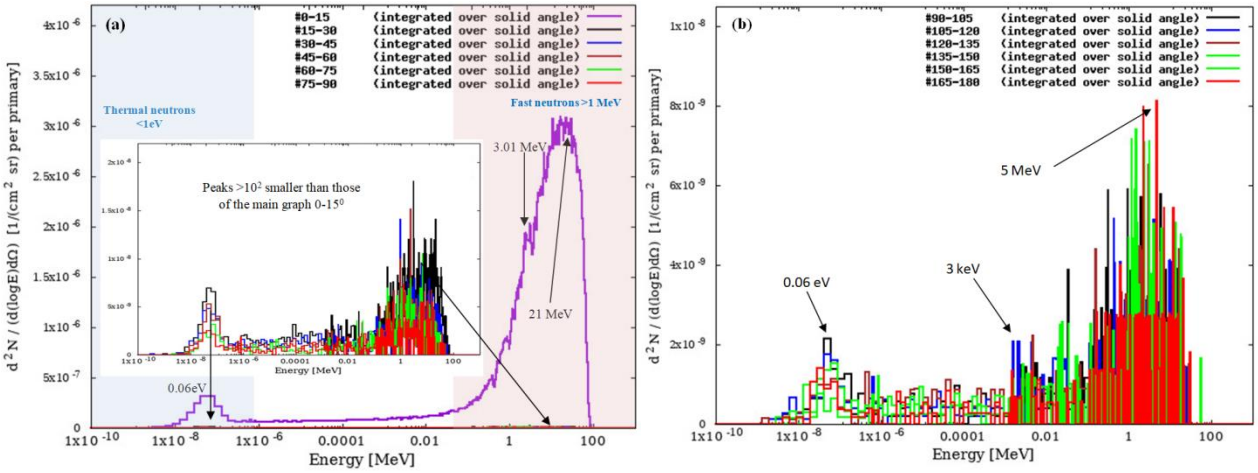

Figure 4. Angular distribution of secondary neutron energy spectra due to 100 MeV primary protons: (a) solid angle regions 00-150 (main graph) 150-300, 300-450, 450-600, 600-750 and 750-900(small graph within), and (b) solid angle regions 900-1050, 1050-1200, 1200-1350, 1350-1500, 1500-1650 and 1650-1800.

Figure 5 displays the 2D neutron fluence (integrated within a solid angle) in (a) ZX-plane, and (b) XY-plane, whereas the incident particles move in Z-direction.

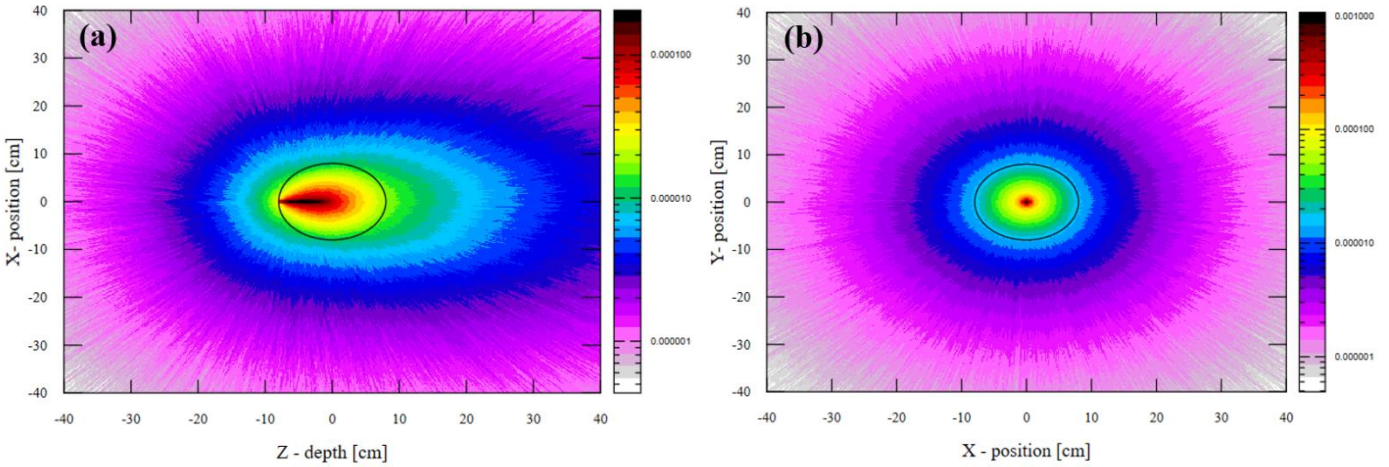

Figure 5. Fluence (integrated within a solid angle) of secondary neutrons upon irradiation with primary protons of 100 MeV in (a) ZX-plane, and (b) XY projection.

Analyzing the neutron fluence with the color scale from Figure 4 one may find that the secondary neutron fluence in the vicinity of the inward periphery of the AHUBO phantom (around the radius of 8 cm) is the range of 10-5 [cm-2], a range that deserves attention when calculating the overall dose from incident particles and those created and absorbed by the patient tissues during the proton therapy.

Simulation of neutron distribution with primary C-ions of 190 MeV/u

Similarly, as was done for protons we have plotted the angular distribution of the energy spectrum of secondary neutrons resulting from the irradiation of the AHUBO phantom head model with 107 primary C-ions. Figure 6 illustrates the double differential angular distributions of the fluence as a function of energy, obtained with USRBDX for angles ranging from 0 to 180 degrees of solid angle, within an angle ranges of 15 degrees.

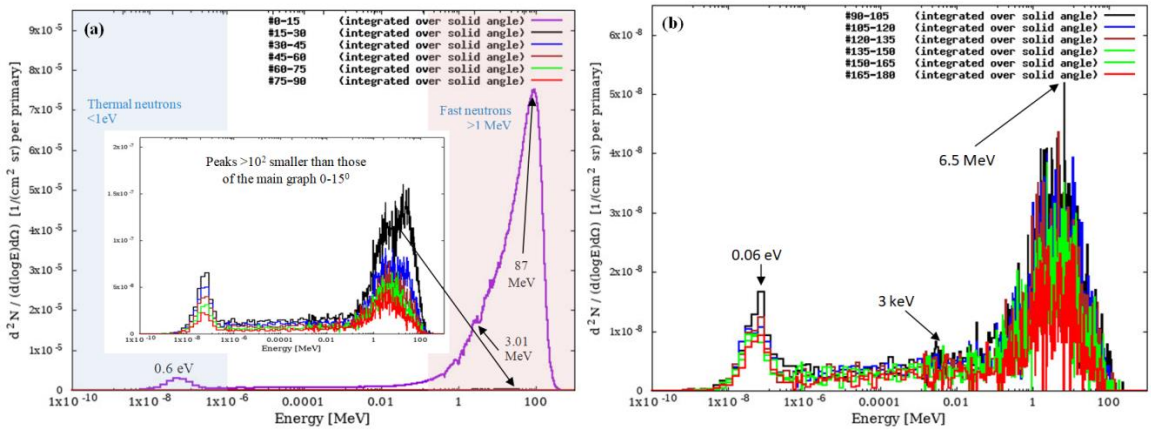

Figure 6. Angular distribution – energy spectrum of the secondary neutrons detected (scored) at different solid angle regions:(a)00-150 (main figure), 150-300, 300-450, 450-600, 600-750 and 750-900 (small figure inside), and (b) solid angle regions 900-1050, 1050-1200, 1200-1350, 1350-1500, 1500-1650 and 1650-1800obtained through the irradiation of AHUBO phantom head model with 106 primary C-ions of 190 MeV/u.

Figure 6 (a) shows the double differential angular distributions for angles ranging from 0 to 90 degrees, which exhibit two prominent peaks. The first neutron peak corresponds to thermal neutrons at 0.6 eV, while the second peak corresponds to fast neutrons with energy of 87 MeV and an overlapping, HE peak at about 3

MeV. In addition to these peaks, there exist intermediate energy continuum neutrons between them showing a tendency to form a peak in the region of about 3 keV. One can notice that the magnitude of the double differential of the neutron fluence spectrum falls for solid angle regions other than 0-15 degrees for over two orders of magnitude. Also, the HE peak shifts towards much lower energies. Figure 6(b) displays the double differential angular distributions for angles ranging from 90 to 180 degrees. As could be seen, the thermal region exhibited a peak at 0.06 eV, energy coinciding with that of the primary protons (Fig 4(a)). In the region of fast neutrons, the maximum energy observed was 6.5 MeV. Additionally, an unpronounced peak with energy of about 3 keV was obtained in the intermediate energy continuum.
Figure 7 displays the neutron fluence generated with 107 primary C-ions with energy of 190 MeV/u. Herein, Figure 7 (a) shows the secondary neutrons fluence integrated within a solid angle in the ZX-plane and (b) in the XY plane. Using the color scale in Figure 7 (b) one can easily estimate the magnitude of the neutron fluence near the margin of the AHUBO phantom (inwards of the area of 8 cm radius- the spherical surface - light blue area) to be around 10-4cm-2.Therange of neutron fluence appears to be one order of magnitude greater than that obtained in case of incident protons.

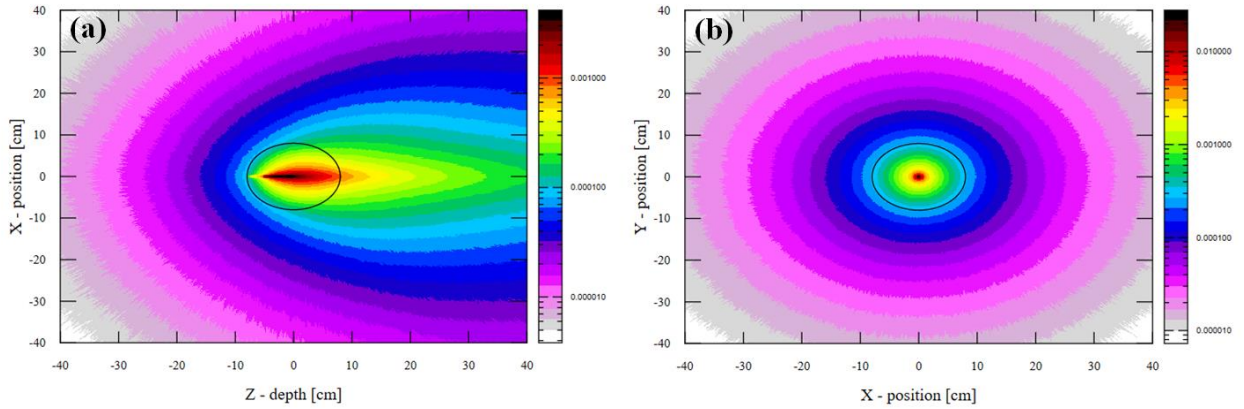

Figure 7. Fluence (integrated within a solid angle) of secondary neutrons upon irradiation with primary protons of 190 MeV/u in (a) ZX-plane, and (b) XY projection.

Conclusions

The AHUBO head was placed in (0, 0, 0) the Cartesian system of the Flair graphical interface of FLUKA, and the ion source at Z=-30 cm apart from the centre. The primary beams consisted of 107 protons of 100 MeV or C-ions of 190 MeV per nucleon, both the energies pertaining to a Bragg peak positioned in the centre of the AHUBO head model (coinciding with the position of the pituitary). In conclusion, we can compare the neutron spectra and their prominent peaks occurring within the solid spatial angles 0-15 degrees with respect to the incident particle direction for the two possible particle therapy modalities (protons and C-ions) as presented in Figure 8. Herein, both treatment modalities reveal the production of thermal neutrons with peak energy of about 0.06 eV and HE peak at about 3 MeV. However, the most pronounced HE neutron peaks occur at different energies, for primary protons at 21 MeV (about 21% of the incident particle energy) and for C-ions at 87 MeV (about 46% of the incident particle energy).

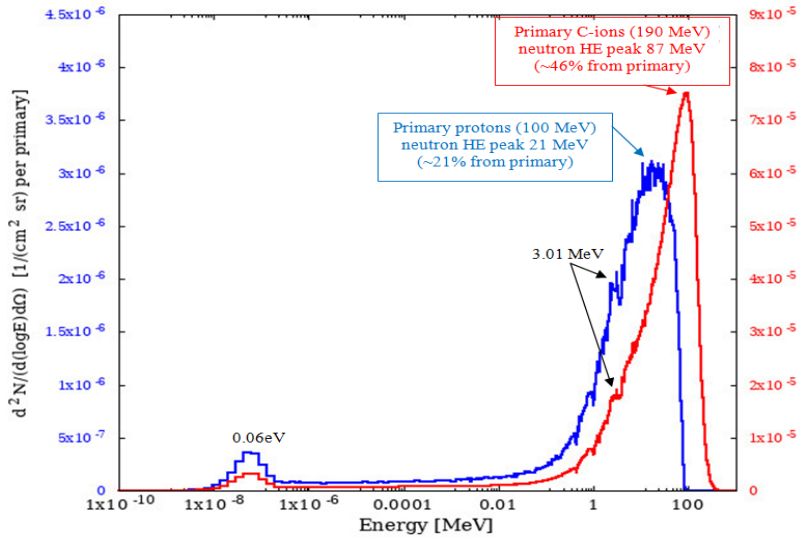

Figure 8. Comparison of neutron spectra for primary C-ions of 190 MeV (red line) and primary protons of 100 MeV (blue line) within a solid angle 0-150 with respect to the direction of the primaries.

In Tables 1 and 2 we have compared the neutron peak energies of the present work with the peaks that could be extracted from the works of other authors for protons and C-ions respectfully.

Table 1. Peak energies in the neutron spectra from proton therapy (100 MeV) and comparison with the results of other authors

No.	Reference	Phantom	Energy of primary protons [MeV]	Peak Energy of thermal neutrons[eV]	Peak Energy of intermediate neutrons[keV]	Peak Energy of HE fast neutrons[MeV]
1	(Howell, 2014)	Patients	250	~0.6	/	~12.5 MeV and ~60 MeV (5% and 24% from E of primary)
2	(MR.Islam , 2013)	Unknown	162	/	~2000	~60 (37% from E of primary)
3	(Y.Zheng, 2007)	Prostate CA-patient	100	/	~300	~30 (30% from E of primary)
4	Present work	AHUBO	100	0.06	/	3 MeV and21 MeV (3% and 21% from E of primary)

Table 2. Peak energies in the neutron spectra from C-ions therapy (190 MeV) and comparison with the results of other authors

No.	Reference	Phantom	Energy of primary C-ions [MeV/u]	Peak Energy of thermal neutrons[eV]	Peak Energy of intermediate fast neutrons[keV]	Peak Energy of HE fast neutrons [MeV/u]
1	(Iwase, 2007)	Water target	200	/	/	~140 (70 % from E of primary)
2	(Kurosawa, 1999)	Patients	400	/	/	~250 (63 % from E of primary)
3	Present work	AHUBO	190	0.06	/	87 (46 % from E of primary)

From Table 1 one may conclude that our simulated neutron spectra with the AHUBO shows similarities with the experimental results, in particularly with the work of Howell et al. (Howell, 2014)where the percentage of the HE peaks pertain to neutrons that carry 5% and 24% of the energy of primary protons, which is comparable to our results (3% and 21%). From Table 2 it is evident that the peaking energy of neutrons due to C-ions is 46% of that of the primaries, which differs substantially from the MC simulations performed by Iwase et al. (Iwase, 2007), 70%, and from the experimental measurements of Kurosawa et al., (Kurosawa, 1999), 63%.

In summary, the angular distribution is affected by several factors, including the energy and type of the incident particle. Finally, the neutron fluence near the margin of the AHUBO (region inwards) for the treatment with primary protons was estimated to be in the range of 10-5cm-2, while in the case of treatment with primary C-ions, 10-4, i.e., one order of magnitude greater. All these findings should be undoubtedly accounted for when calculating the total dose absorbed by the patient during the C-ion cancer treatment.

Recommendation

The limitations of the study are from the lack of access to experimental equipment in which the accelerated primary particles (protons and C-ions) in the particle therapy energy range are targeting an actual AHUBO phantom, to be able to compare our Monte-Carlo simulation results with the experimental results performed with actual detectors. It is also recommended that future simulations should be run with 108 primaries.

References

[1]. Baskar, R. a.-W. (2012). Cancer and radiation therapy: current advances and future directions. International journal of medical sciences , 9 (3), 193.

[2]. Battistoni, G. a. (2007). The FLUKA code: Description and benchmarking. AIP Conference proceedings , 896, 31--49.

[3]. Bexheti, R. I.-,. (2023). Applited Radiation and Isotops, Submitted for publication.

[4]. Chetty, I. J.-M. (2007). Report of the AAPM Task Group No. 105: Issues associated with clinical implementation of Monte Carlo-based photon and electron external beam treatment planning. Medical physics , 34 (12), 4818--4853.

[5]. Cooper, N. (1987). os Alamos Science Number 15: Special Issue on Stanislaw Ulam 1909-1984. Los Alamos National Lab.(LANL), Los Alamos, NM (United States).

[6]. De Saint-Hubert, M. F. (2022). The influence of nuclear models and Monte Carlo radiation transport codes on stray neutron dose estimations in proton therapy. Radiation Measurements (150), 106693.

[7]. Fasso, A. a. (2003). The physics models of FLUKA: status and recent development. arXiv preprint hep-ph/0306267

[8]. Howell, R. B. (2014). Secondary neutron spectrum from 250-MeV passively scattered proton therapy: Measurement with an extended-range Bonner sphere system. Medical physics , 41 (9), 092104.
[9]. Islam, M. C. (2013). Off-axis dose equivalent due to secondary neutrons from uniform scanning proton beams during proton radiotherapy. Physics in Medicine \& Biology , 58 (22), 8235.
[10]. Iwase, H. a.-M. (2007). Experimental and theoretical study of the neutron dose produced by carbon ion therapy beams. Radiation protection dosimetry , 126 (1-4), 615--618.
[11]. Janz, N. K. (2004). Patient-physician concordance: preferences, perceptions, and factors influencing the breast cancer surgical decision. Journal of clinical oncology , 22 (15), 3091-3098.
[12]. Jones, B. a. (2005). Particle Therapy Co-operative Oncology Group (PTCOG 40) Meeting, Institute Curie 2004. The British journal of radiology , 78 (926), 99-102.
[13]. Kalos, M. H. (2009). Monte carlo methods. John Wiley \& Sons.
[14]. Kurosawa, T. a. (1999). Measurements of secondary neutrons produced from thick targets bombarded by high-energy helium and carbon ions. Nuclear Science and Engineering , 132 (1), 30--57.
[15]. Lindborg, L. H. (2013). Lineal energy and radiation quality in radiation therapy: model calculations and comparison with experiment. Physics in medicine \& Biology , 58 (10), 3089.
[16]. M. Dosanjh, R. M. (2022). Availability of technology for managing cancer patients in the Southeast European (SEE) region. Clinical and Translational Radiation Oncology , 34, 57--66.
[17]. M.M. Ristova, V. G. (2021). Patients with cancer in the countries of south-east europe (the Balkans) region and prospective of the particle therapy center: South-East European International Institute for Sustainable Technologies (SEEIIST). Advances in Radiation Oncology , 6 (6), 100772.
[18]. MR.Islam, M. a. (2013). Off-axis dose equivalent due to secondary neutrons from uniform scanning proton beams during proton radiotherapy. Physics in Medicine \& Biology , 58 (22), 8235.
[19]. Paganetti, H. a. (2002). Relative biological effectiveness (RBE) values for proton beam therapy. International Journal of Radiation Oncology* Biology* Physics , 53 (2), 407--421.
[20]. Parodi, K. a. (2007). Clinical CT-based calculations of dose and positron emitter distributions in proton therapy using the FLUKA Monte Carlo code. Physics in Medicine \& Biology , 52 (12).
[21]. Pia, M. G. (2010). Physics-related epistemic uncertainties in proton depth dose simulation. . IEEE Transactions on Nuclear Science, , 57(5), 2805-2830.
[22]. R.I.-Bexheti, M. R. (2020). State-of-the-art and the future of particle therapy (perspectives for SEE countries). Physics AUC , 30 (part II), 246--262.
[23]. Schulz-Ertner, D. a. (2007). Particle radiation therapy using proton and heavier ion beams. Journal of clinical oncology , 25 (8), 953--964.
[24]. U. Amaldi, E. B. (2021). South East European International Institute for Sustainable Technologies (SEEIIST). Frontiers in Physics , 8, 567466.
[25]. Y.Zheng, Y. a. (2007). Monte Carlo simulations of neutron spectral fluence, radiation weighting factor and ambient dose equivalent for a passively scattered proton therapy unit. Physics in Medicine \& Biology , 53 (1), 187.